Electronic Supplementary Information (ESI)

New insight on intramolecular conjugation in the design of efficient blue materials: from the control of emission to absorption

Jie Yang[†,#], Qingxun Guo[‡,#], Zichun Ren[†], Xuming Gao[†], Qian Peng[§], Qianqian Li[†], Dongge Ma[‡,*], and Zhen Li[†,*]

[†]Department of Chemistry, Hubei Key Lab on Organic and Polymeric Opto-Electronic Materials, Wuhan University, Wuhan 430072, China. Fax: (86)27-68756757. E-mail: lizhen@whu.edu.cn; lichemlab@163.com.

[‡]Changchun Institute of Applied Chemistry, The Chinese Academy of Sciences Changchun 130022, China. E-mail: mdg1014@ciac.jl.cn.

[§]Key Laboratory of Organic Solids, Beijing National Laboratory for Molecular Science (BNLMS), Institute of Chemistry, Chinese Academy of Sciences, 100190 Beijing, China.

[#] These authors contributed equally to this work.

Table of Contents

(λ_{EL}), external quantum yields (EQE) of TPA-3TPP, TTPECaP, Cz-3tPE, Cz-3TPP and the responding different λ_{abs} and λ_{EL} effects.

Figure S10 The PL spectra in THF/n-hexane mixtures with different n-hexane fractions: **(A)** Cz-3tPE, concentration ≈ 10 μM; excitation wavelength 330 nm; **(B)** TPA-3TPP, concentration ≈ 10 μM; excitation wavelength 340 nm; **(C)** Cz-3TPP, concentration ≈ 10 μM; excitation wavelength 310 nm.

Figure S11 Calculated molecular orbital amplitude plots of HOMO and LUMO levels and optimized molecular structures of Cz-3tPE, TPA-3TPP and Cz-3TPP.

Figure S12 The cyclic voltammograms of Cz-3tPE, TPA-3TPP and Cz-3TPP recorded in dichloromethane.

Figure S13 The changes in power efficiency with the current density.

Figure S14 MALDI-TOF of Cz-3tPE.

Figure S15 MALDI-TOF of TPA-3TPP.

Figure S16 MALDI-TOF of Cz-3TPP.

Experimental Section

Characterizations

^{1}H and ^{13}C NMR spectra were conducted on a Mecuryvx300 or Ascend 400 MHz spectrometer. Elemental analyses of carbon, hydrogen and nitrogen were taken on a Carlo-Erba-1106 microanalyzer. Mass spectra were measured on a Voyager DESTR MALDI-TOF mass spectrometer. UV-Vis absorption spectra were measured on a Shimadzu UV-2500 recording spectrophotometer. Photoluminescence spectra were recorded on a Hitachi F-4600 fluorescence spectrophotometer. Differential scanning calorimetry (DSC) was performed on a NETZSCHDSC 200 PC instrument from room temperature to 300 ^{o}C at a heating rate of 15 ^{o}C min^{-1} under argon. Thermogravimetric analysis (TGA) was measured on a NETZSCH STA 449C instrument. The thermal stabilities of the samples under a nitrogen atmosphere were determined by measuring their weight loss while heating from room temperature to 700 ^{o}C at a rate of 15 ^{o}C min^{-1}. Cyclic voltammetry (CV) was carried out on a CHI voltammetric analyzer in three electrode cells with a platinum counter electrode, an Ag/AgCl reference electrode, and a glassy carbon working electrode at a scan rate of 100 mV s^{-1} in anhydrous dichloromethane solution with 0.1 M tetrabutylammonium perchlorate as the supporting electrolyte and purged with nitrogen. The potentials obtained in reference to the Ag/Ag^{+} electrode were converted into values versus the saturated calomel electrode (SCE) by means of ferrocenium/ferrocene (Fc^{+}/Fc) standard. Fluorescence quantum yields of powders and THF solutions were determined with a HamamatsuC11347 Quantaurus-QY absolute fluorescence quantum yield spectrometer.

Solvatochromic effect

The influence of solvent environment on the optical property of our compounds can be understood using the Lippert-Mataga equation:

$$v_a - v_f = \frac{1}{4\pi\varepsilon_0} * \frac{2\Delta\mu^2}{hca^3}\Delta f + Const.$$

where $a = \sqrt[3]{\frac{3M}{4\pi d N_a}}$

In the above equations, v_a-v_f is the Stokes shift, ε_0 is the vacuum permittivity, h is Planck's constant, c is the velocity of light, a is the Onsager radius of fluorophore, $\Delta\mu = \mu_e - \mu_g$ is the difference in the dipole moment of fluorophore between the excited (μ_e) and the ground (μ_g) states, e and n are the static dielectronic constant and the refractive index of the solvent, respectively, Δf is the orientation polarizability, M is the molecular weight, d is the density of molecule, and N_a is Avogadro's number. Therefore, based on equation, the change in dipole moment, $\Delta\mu = \mu_e - \mu_g$, can simply be estimated from the slope of a plot of v_a-v_f against Δf.

Computational details

The molecular structures, orbital distributions of HOMO and LUMO energy levels and the ground state dipole moments (μ_g) were optimized at B3LYP/6-31g* level using Gaussian 09 program.

The hole-only devices and measurement

The hole-only devices were fabricated on glass substrates. Prior to deposition, the substrate was thoroughly cleaned in an ultrasonic bath using subsequently detergents and deionized water. The structures of devices were ITO/MoO_3/Cz-3tPE or TPA-3TPP or Cz-3TPP (110 nm)/MoO_3/Al, and layers, Cz-3tPE, TPA-3TPP and Cz-3TPP, were grown in succession by thermal evaporation without breaking vacuum (10^{-5} Pa). Here, the interfacial layer MoO_3 worked as hole-injection and electron-blocking layers. The Al electrodes were deposited on the substrates through shadow masks. The current-voltage (I–V) characteristics were carried out using a Keithley 2400 sourcemeter integrated with a vacuum cryostat (Optistat DN-V, Oxford Instruments). The admittance was measured at room temperature by using an Agilent E4980A precision LCR meter in the frequency range of 20 Hz–13 MHz with the oscillation amplitude of the ac voltage kept at 100 mV.

OLED devices and measurement

The hole-transporting material of NPB (1,4-bis(1-naphthylphenylamino)-biphenyl), electron blocking material of 1,3-Di-9-carbazolylbenzene (MCP) and electron transporting materials of 1,3,5-tris(N-phenylbenzimidazol-2-yl)benzene (TPBi) and 1,3,5-tri[(3-pyridyl)-phen-3-yl]benzene (TmPyPB) were obtained from a commercial source. The EL devices were fabricated by vacuum deposition of the materials at a base pressure of 10^{-5} Torr onto glass pre-coated with a layer of indium tin oxide (ITO) with a sheet resistance of 25 Ω per square. Before deposition of an organic layer, the clear ITO substrates were treated with oxygen plasma for 2 min. The deposition rate of organic compounds was 1–2 Å s^{-1}. Finally, a cathode composed of lithium fluoride (1 nm) and aluminium (100 nm) was sequentially deposited onto the substrate in the vacuum of 10^{-5} Torr. The *L–V–J* of the devices was measured with a Keithey 2400 Source meter and a Keithey 2000 Source multimeter equipped with a calibrated silicon photodiode. The EL spectra were measured by JY SPEX CCD3000 spectrometer. All measurements were carried out at room temperature under ambient conditions.

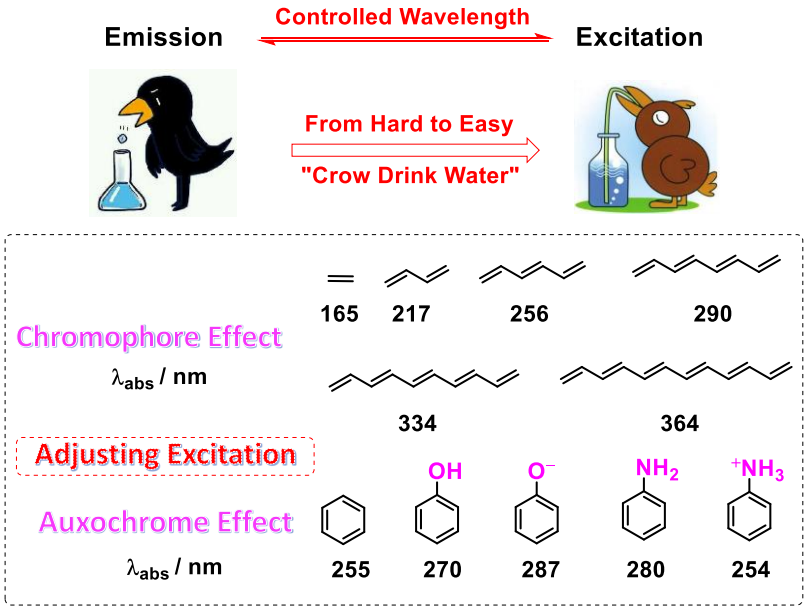

Figure S1 A new sight on the intramolecular conjugation in the design of efficient blue materials—from the control of emission to absorption: the chromophore effect (the maximum absorption wavelengths increase with the addition of double bond, nearly 30 nm per double bond) and auxochrome effect (the maximum absorption wavelengths increase with the enhanced electron donating ability for auxochrome) on adjusting the maximum absorption wavelength (λ_{abs}).

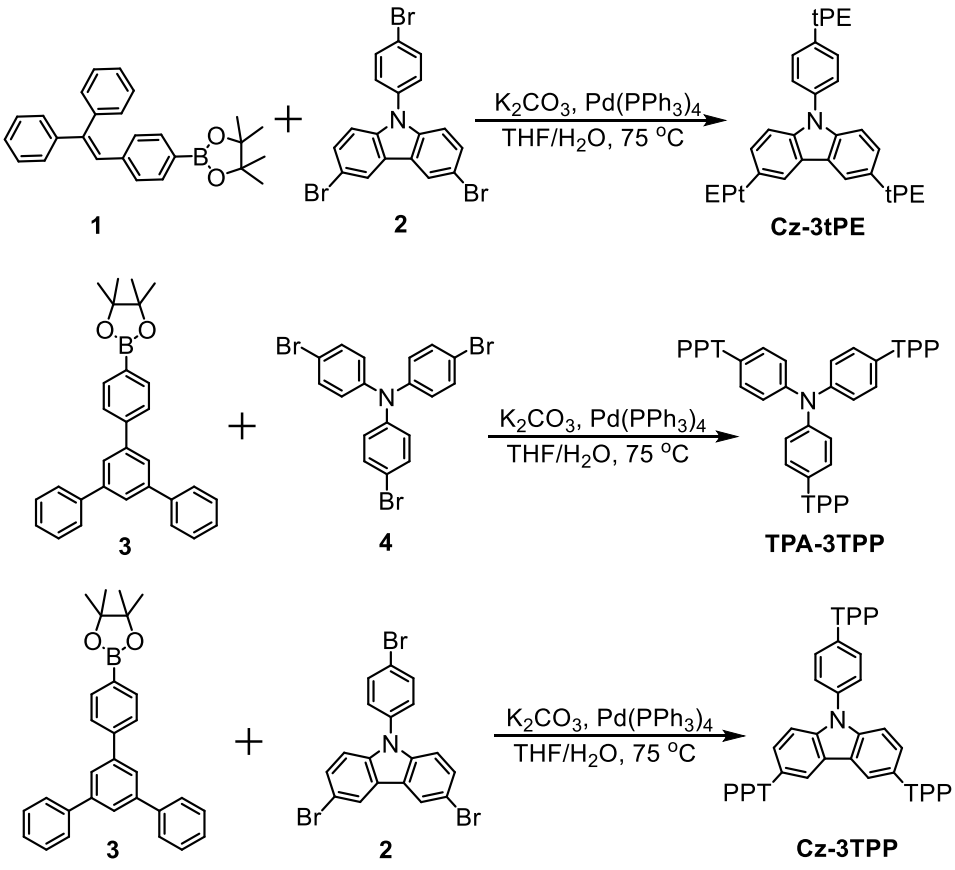

Scheme S1 The synthetic routes to Cz-3tPE, TPA-3TPP and Cz-3TPP.

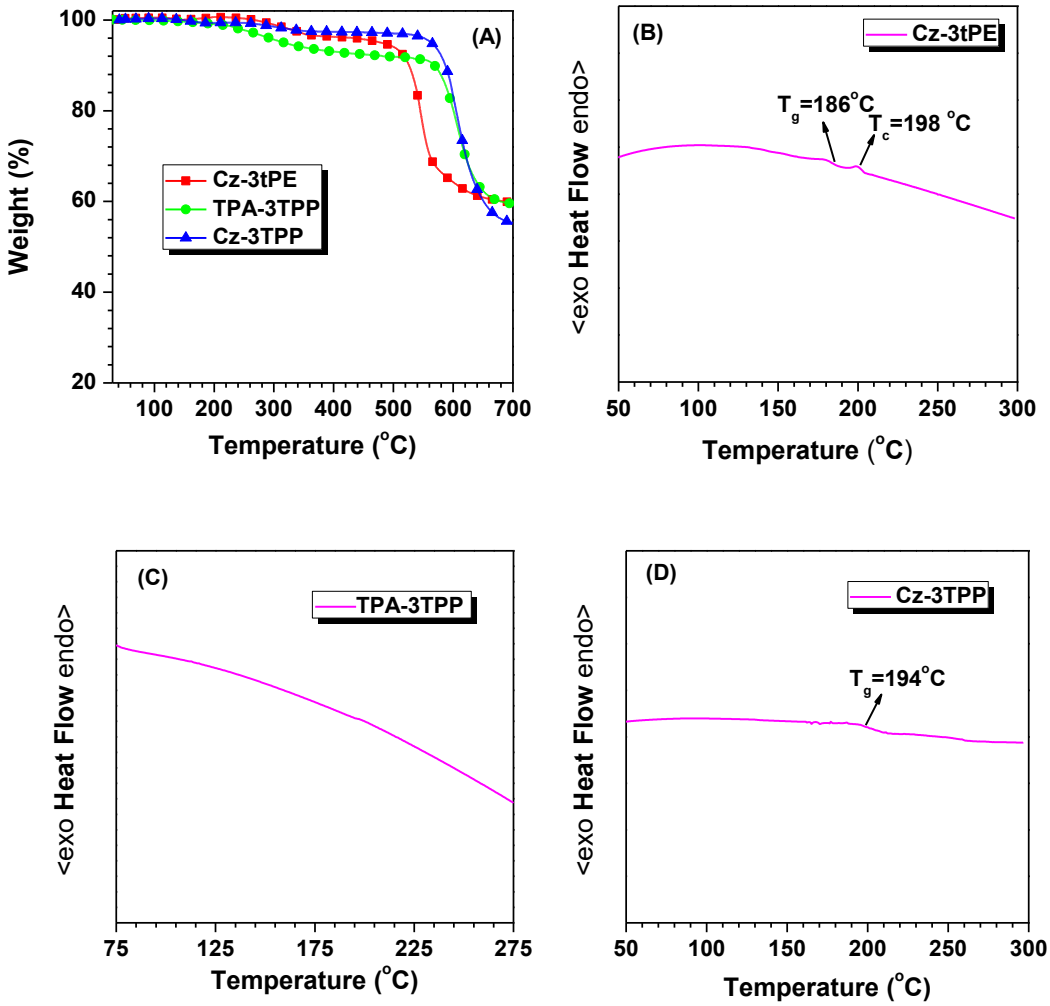

Figure S2 TGA curves **(A)** and DSC curves (**B**, **C**, **D**) for Cz-3tPE, TPA-3TPP and Cz-3TPP recorded under N_2 at a heating rate of 15 °C/min.

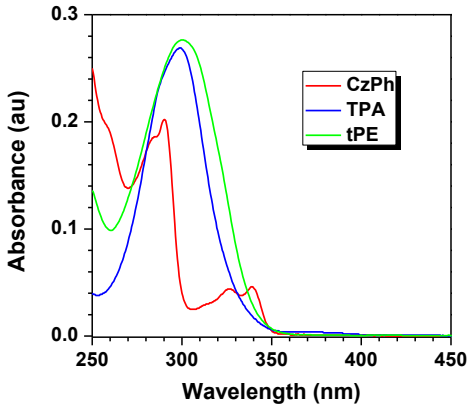

Figure S3 UV-vis spectra of CzPh, TPA and tPE in THF solution (concentration ≈ 10 μM).

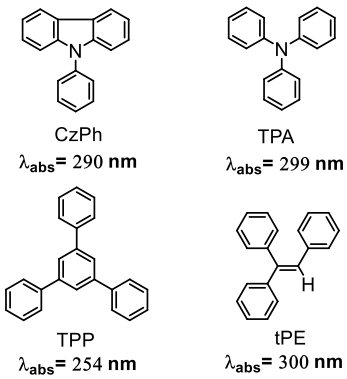

Figure S4 The chemical structures and the corresponding maximum absorption wavelengths (λ_{abs}) for CzPh, TPA, TPP and tPE.[1]

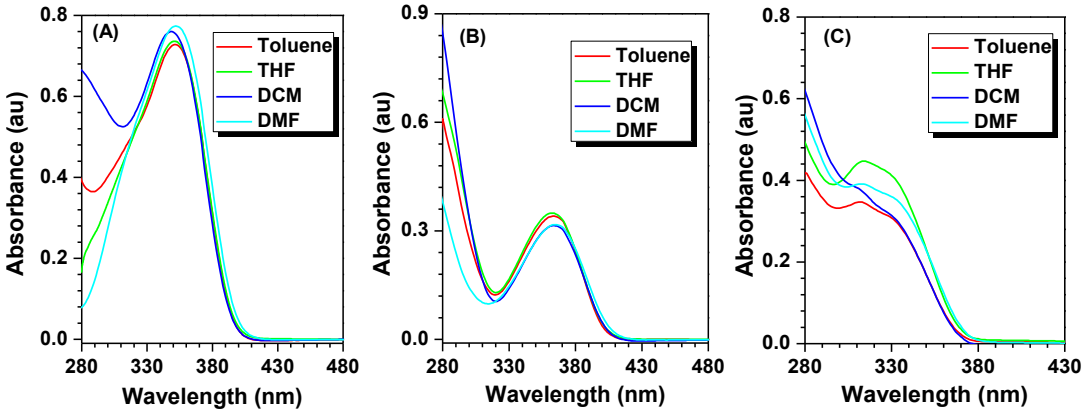

Figure S5 (A) UV-vis spectra of Cz-3tPE in different solutions, concentration ≈ 10 μM; **(B)** UV-vis spectra of TPA-3TPP in different solutions, concentration ≈ 10 μM; **(C)** UV-vis spectra of Cz-3TPP in different solutions, concentration ≈ 10 μM.

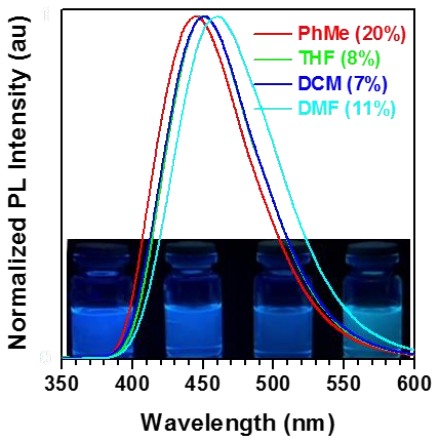

Figure S6 PL spectra in different solutions and the corresponding quantum yields for Cz-3tPE, concentration ≈ 10 μM.

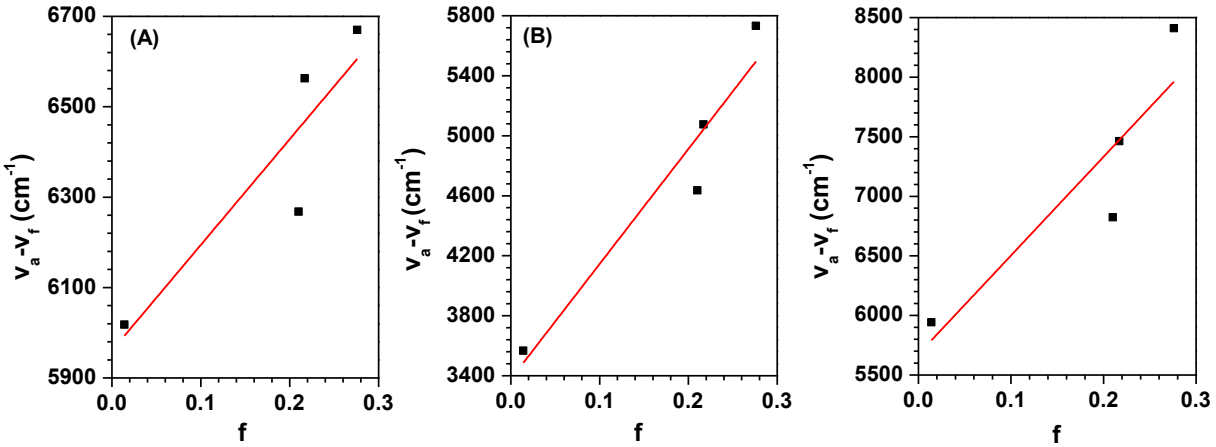

Figure S7 Linear correlation of orientation polarization (*f*) of solvent media with the Stokes shift (υ_a–υ_f; a: absorbed light; f: fluorescence) for Cz-3tPE (A), TPA-3TPP (B) and Cz-3TPP (C).

Table S1 Detailed absorption and emission peak positions of Cz-3tPE, TPA-3TPP and Cz-3TPP in different solvents and the calculated ground-state dipole moment (μ_g), excited state dipole moment (μ_e).

Compounds	Solvents	*f*	λ_a (nm)	λ_f (nm)	v_a-v_f (cm^{-1})	μ_g [a] (D)	μ_e [b] (D)
Cz-3tPE	PhMe	0.014	351	445	6018	3.3	12.9
	THF	0.210	351	450	6268		
	DCM	0.217	348	451	6563		
	DMF	0.276	352	460	6670		
TPA-3TPP	PhMe	0.014	363	417	3567	0.1	18.8
	THF	0.210	362	435	4636		
	DCM	0.217	363	445	5076		
	DMF	0.276	364	460	5733		
Cz-3TPP	PhMe	0.014	312	383	5942	2.9	22.3
	THF	0.210	313	398	6823		
	DCM	0.217	311	405	7643		
	DMF	0.276	312	423	8411		

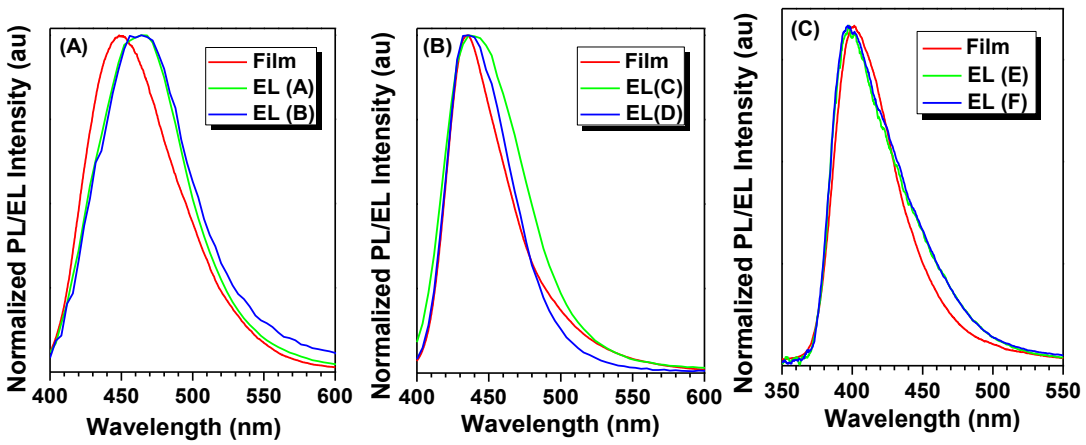

Figure S8 PL spectra of films and EL spectra for Cz-3tPE **(A)**, TPA-3TPP **(B)** and Cz-3TPP **(C)**, respectively. Device configurations for EL (A) and EL (C): ITO/MoO_3/NPB (50 nm)/MCP (10

nm)/Cz-3tPE or TPA-3TPP (15 nm)/TPBi (35 nm)/LiF/Al; Device configurations for EL (B), EL (D) and EL (E): ITO/MoO_3/Cz-3tPE or TPA-3TPP or Cz-3TPP (75 nm)/TPBi (35 nm)/LiF/Al; Device configuration for EL (F): ITO/MoO_3/Cz-3TPP (75 nm)/TmPyPB (35 nm)/LiF/Al.

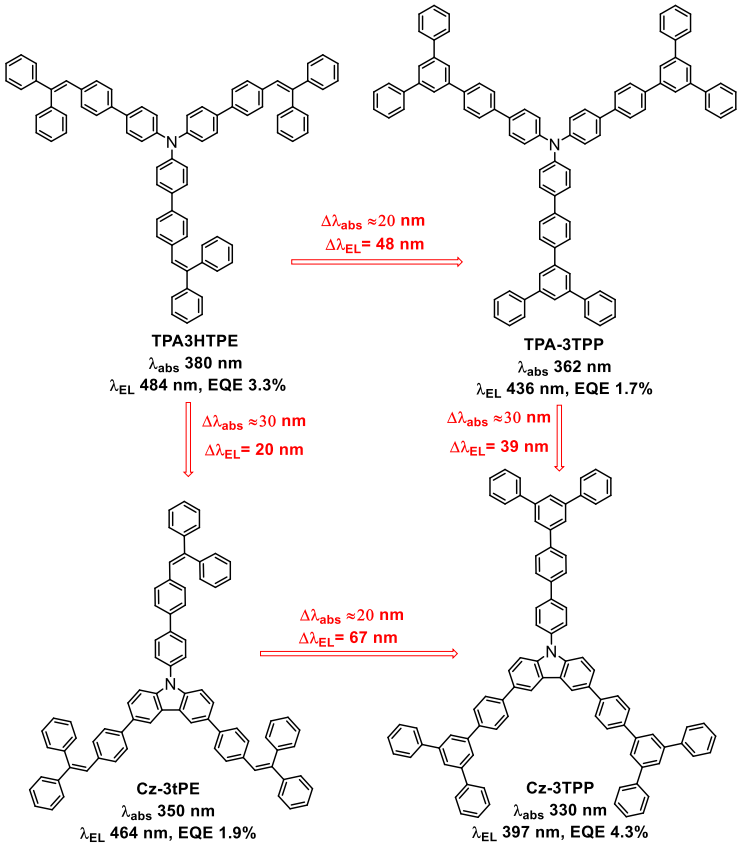

Figure S9 The chemical structures, maximum absorption wavelengths (λ_{abs}), EL emission peaks (λ_{EL}), external quantum efficiencies (EQE) of TPA-3TPP, TTPECaP, Cz-3tPE, Cz-3TPP and the corresponding different λ_{abs} and λ_{EL} effects (Note: Cz-3tPE, Cz-3TPP and TPA-3TPP were reported in this paper, and TPA3HTPE was reported in reference 2).

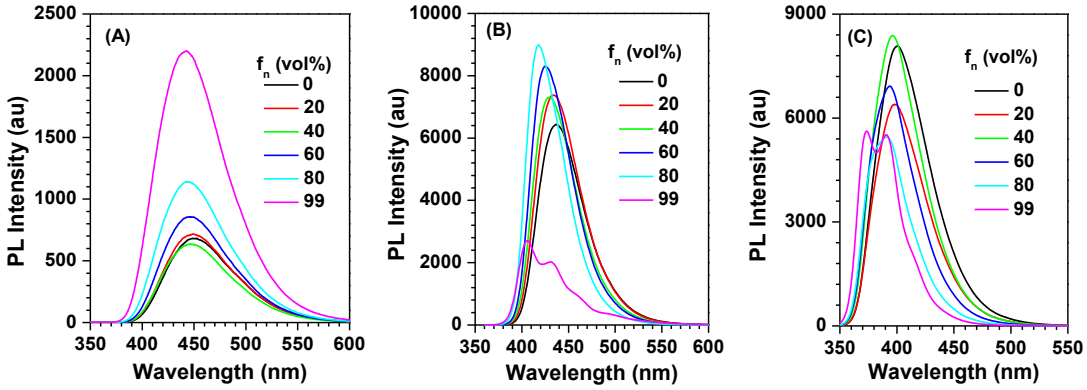

Figure S10 PL spectra in THF/*n*-hexane mixtures with different *n*-hexane fractions: **(A)** Cz-3tPE, concentration ≈ 10 μM; excitation wavelength 330 nm; **(B)** TPA-3TPP, concentration ≈ 10 μM; excitation wavelength 340 nm; **(C)** Cz-3TPP, concentration ≈ 10 μM; excitation wavelength 310 nm.

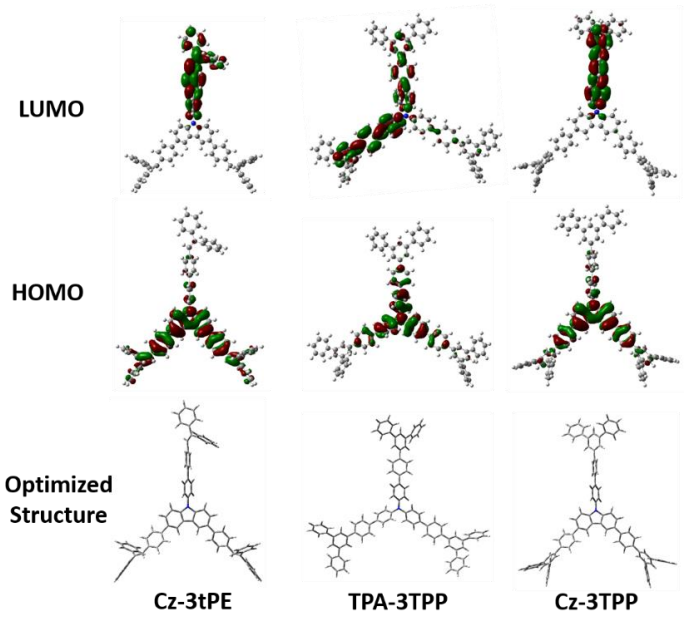

Figure S11 Calculated molecular orbital amplitude plots of HOMO and LUMO levels and optimized molecular structures of Cz-3tPE, TPA-3TPP and Cz-3TPP.

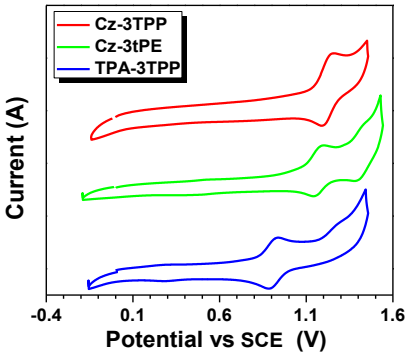

Figure S12 The cyclic voltammograms of Cz-3tPE, TPA-3TPP and Cz-3TPP recorded in dichloromethane.

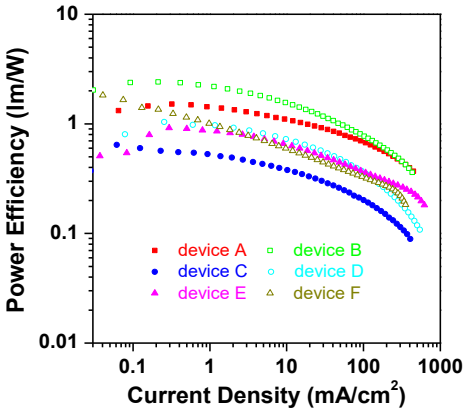

Figure S13 The changes in power efficiency with the current density. Device configurations for A and C: ITO/MoO_3/NPB (50 nm)/MCP (10 nm)/Cz-3tPE or TPA-3TPP (15 nm)/TPBi (35 nm)/LiF/Al; Device configurations for B, D and E: ITO/MoO_3/Cz-3tPE or TPA-3TPP or Cz-3TPP (75 nm)/TPBi (35 nm)/LiF/Al; Device configuration for F: ITO/MoO_3/Cz-3TPP (75 nm)/TmPyPB (35 nm)/LiF/Al.

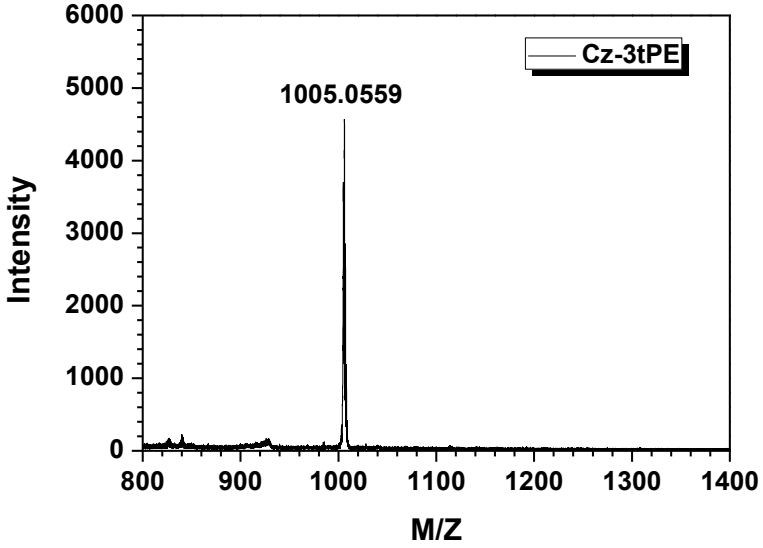

Figure S14 MALDI-TOF of Cz-3tPE.

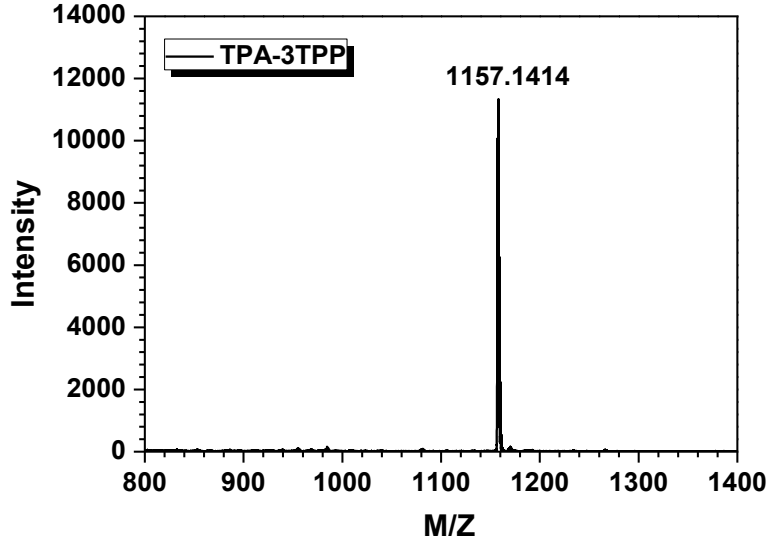

Figure S15 MALDI-TOF of TPA-3TPP.

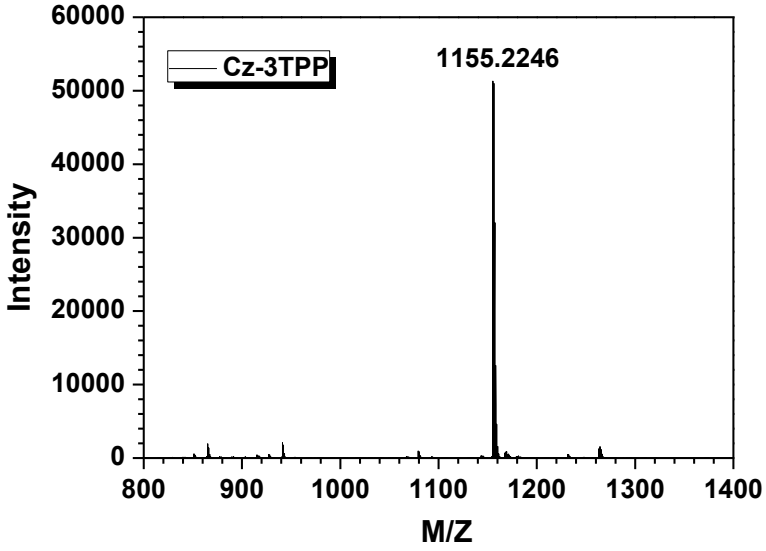

Figure S16 MALDI-TOF of Cz-3TPP.

Reference

1 V. Vergadou, G. Pistolis, A. Michaelides, G. Varvounis, M. Siskos, N. Boukos and S. Skoulika, *Cryst. Growth Des.,* 2006, **6**, 2486.

2 G. Chen, W. Li, T. Zhou, Q. Peng, D. Zhai, H. Li, W. Yuan, Y. Zhang and B. Z. Tang, *Adv. Mater.,* 2015, **27**, 4496.